European Journal of Wood and Wood Products (2023) 81:45–58
https://doi.org/10.1007/s00107-022-01861-z

ORIGINAL ARTICLE

Wood fiber - sodium silicate mixtures for additive manufacturing of composite materials

Berlinda O. Orji[1] · Conal Thie[2] · Kenneth Baker[3] · Michael R. Maughan[2] · Armando G. McDonald[1]

Received: 25 January 2022 / Accepted: 23 June 2022 / Published online: 2 August 2022

Abstract

A composite mixture of wood fiber and sodium silicate (SS) binder has been explored as a viable material for use in additive manufacture of wood based composite materials. Mixtures of 50–60% wood fiber and 50 – 40% SS were explored. The curing behavior of these formulations were examined by differential scanning calorimetry (DSC) and dynamic rheometry. An exothermic curing peak of 83 °C was observed for SS and increased to 153 and 163 °C with the addition of wood fiber. Rheology flow curves showed higher viscosity values for 50/50 blends and lower values for SS. A custom extrusion system was fabricated and 50/50 wet blends were extruded, cured at different temperatures, and characterized for flame retardancy, mechanical, thermal, and water absorption properties. Surface chemistry changes before and after curing were determined by Fourier Transform Infrared (FTIR) spectroscopy. Mechanical properties, determined by three-point bend testing, improved with the addition of the wood fiber but varied with different curing temperatures and thermal stability of the composites increased with curing temperature. This extruded wood-SS composite shows promise for use in additive manufacturing.

1 Introduction

Sawmill residues (sawdust and planar shavings) is a useful resource that can be utilized as a sustainable feedstock and in the U.S.A, 83.4 million tons of primary timber wood residues were generated in 2010 and 85% was used in wood composites (Falk and McKeever 2012). Waste wood is also commonly used in composite wood panels (particleboard) and composite decking (wood plastic composites) (Cherkasova 2020). The production of composite panels requires binders which are mostly synthetic resins (urea-formaldehyde and phenol-formaldehyde) that require curing in a heated press and can release formaldehyde emissions which pose environmental and health risks (Papadopoulos 2020; Antov et al. 2020). Studies have implemented the use of wood residues and different matrix in additive manufacturing using different fabrication processes, however, using high content wood residues with thermosets has not been widely explored (Buschmann et al. 2021; Krapež Tomec and Karič 2022; Rosenthal et al. 2018).

The global additive manufacturing and materials market was $12.8 billion in 2018 and is expected to grow annually by 25% by 2023 (Additive Manufacturing Materials Market – Industry Reports, 2019). This expansion has been driven by rapid advancements in materials used, new additive manufacturing technologies, and shifting from prototyping to parts fabrication. This process typically involves a layer-by-layer deposition process which is repeated until the part is created. The most common and known form

The original online version of this article was revised due to incorrect figure 5.

✉ Armando G. McDonald
armandm@uidaho.edu

[1] Forest and Sustainable Products Program, Department of Forest, Rangeland and Fire Sciences, University of Idaho, 83844 Moscow, ID, USA

[2] Department of Mechanical Engineering, University of Idaho, 83844 Moscow, ID, USA

[3] Integrated Design Laboratory, University of Idaho, 83702 Boise, ID, USA

of additive manufacturing is fused filament fabrication or fused deposition modeling (Mazzanti et al. 2019). A new method of 3-dimensional (3D) printing called fused particle fabrication or fused granular fabrication uses thermoplastic powders/pellets that feed into an extruder that produces a filament *in-situ* for printing (Whyman et al. 2018). This process can also form composite materials by combining reinforcing particles/fibers and plastic waste to form components but via a melt process (Woern et al., 2018). An alternative method of additive manufacturing involves the use of a liquid resin-based 3D printing that uses UV-light curing (stereolithography and digital light processing) and this has been applied to high-resolution printing applications, however the resins used are expensive (Bagheri and Jin 2019). Ming et al. (2019) had produced epoxy-continuous fiber composites but also required high temperature curing. For construction applications, cement-based 3D printing systems have been used but require long curing times of 28 days and have high embodied energy (Rahul et al. 2019). There is a gap in additive manufacturing technology to produce low temperature cured, formaldehyde free, inorganic based thermoset resin-wood composite materials.

Sodium silicate (SS), also known as water glass, is an example of an inorganic binder used due to its eco-friendly nature, affordability, ease to handle and prepare, high strength, weather resistance, and flame retardant properties (Dimas et al. 2009). It is commonly used in thermal insulation, as a binder for sand-cast molding in foundries, and to modify natural fiber surfaces (Chen et al. 2018; Mamun and Arifuzzaman 2020; Chai et al. 2021; Owusu 1982). SS has been impregnated into solid wood lumber and wood surface treatments to protect wood from biodegradation, improve its physical, mechanical and flammability properties (Peng et al. 2010; Pratheep Kumar et al. 2015; Ming-Li et al. 2019). Composites made with natural fibers like sugarcane bagasse, hemp fiber, coconut, raffia palm, and sisal using SS as binder have been produced and resulted in materials with improved mechanical properties (Ng et al. 2018; Bifulco et al. 2020; Korniejenko et al. 2016).

Studies have shown that the curing of SS can be attained using different methods including the use of alkali activators like sodium hydroxide or potassium hydroxide, use of weak acids, catalysts, the removal of water through heating, the use of carbon dioxide (CO_2), and the use of liquid ester hardeners (Owusu 1982; Mazhirin 2002). SS acts as a binder through its formation of silicate, silicic acid, and precipitated gel bonds when cured. The gel further stiffens into a solid "glass" due to the water molecules which are drawn and adsorbed to the surface of the gel and the crosslinking and polymerization of the solid material into complex chains and networks (Sarmin et al. 2014; Brown 2000). Although the use of SS is common in various applications, a limited number of studies on the rheology, thermal properties and curing of SS in the presence of wood fiber have been documented (Pham and Hatzignatiou 2016; Katoueizadeh et al. 2020).

The aim of this study was to explore the use of SS with wood fiber from sawmill residues to produce an extruded wood composite material. The study explored the mixing, formulation, and effect of wood particle size and composition on composite properties. Curing behavior was determined by differential scanning calorimetry (DSC) and dynamic rheology. The rheology of a wood-SS paste was determined by a combination of dynamic and capillary rheology. The wood-SS paste was extruded into rod for studying the influence of curing temperature on flexural properties of the composite. The thermal stability of the composites was determined by thermogravimetric analysis (TGA) and a flame test.

2 Materials and methods

2.1 Materials

Sawmill residues were obtained from Plummer Forests Products, Post Falls, ID., USA. Wood residues (100 g batches) were screened using 40 mesh standard US screen, collected, and pooled together. Commercial SS solution (37 wt%, ThermoFisher Scientific, Waltham, MA, USA), pH 12.5, 1.39 g/cm^3 at 20 °C, was used as received.

2.2 Composite preparation

Wood fiber moisture content was determined using a HB43-S Halogen Moisture Analyzer (Mettler Toledo, Columbus, OH, USA) for 2.6 to 3.5 g of samples in triplicate.

Screened 40 mesh (≤ 0.425 mm) wood fiber and SS were mixed in ratio of 50:50 and 60:40 ratio on a dry weight basis taking into account the wood moisture content and the SS solids content. Small batches (2 g total weight) were mixed (30 s) using an herb grinder (Fig.S1 in Supplementary Information) for dynamic rheology tests and larger batches (200 g total weight) were mixed (1–2 min) using food processor (Hamilton Beach model 70730 (450 W, 10 cup capacity)), (Fig. S2 in Supplementary Information) for capillary rheometry and extrusion studies.

2.3 Sample characterization

Wood fiber morphology (length and width) was determined on 400 particles by optical microscopy (Olympus BX51 microscope with a DP70 digital camera at 40x, San Diego, CA, USA). Images were analyzed using Fiji ImageJ

software (version 2.1.0/1.53c, Java 1.8.0_172 (64bit)). Sieve analysis was performed on 100 g of the screened 40 mesh wood fibers for 10 min using a standard shaker to pass through 40, 60, 80, 100 and 200 US standard mesh screens. Sieve analysis was performed in triplicate and the total weight of samples between sieves was determined and the cumulative percent weight was determined to ascertain size distribution.

Wet and cured extruded wood-SS blends were analyzed (in triplicate) by Fourier transform infrared (FTIR) spectroscopy using a Nicolet-iS10 spectrometer (64 scans, Thermo-Scientific, Madison, WI, USA) with an attenuated total reflectance (ATR) accessory (Smart Orbit, Diamond). The spectra were baseline and ATR corrected and averaged using the Omnic v9.8.3 software.

2.4 Thermal analysis

Each blended wood-SS formulation was freeze-dried prior to DSC analysis since the presence of water had a peak due to evaporation that coincided with that of the curing peaks. To improve sensitivity of traditional DSC, modulated DSC (MDSC) experiments were performed, in quadruplet, on blends (5 mg – 10 mg) using a Q200 DSC (TA instruments, New Caste, DE, USA) under nitrogen (20 mL/min) and refrigerated cooling. Samples were equilibrated at 40 °C, modulated at ± 3.183 °C for 60 s, kept isothermal for 2 min and ramped from 40 to 200 °C, at a heating rate of 10 °C/min. Data was analyzed using the TA Universal analysis software.

Thermal degradation and curing behavior of wet and cured wood-SS blends under different curing regimes were determined in triplicate using a Perkin-Elmer TGA-7 instrument (Shelton, CT, USA) under nitrogen (30 mL/min). Isothermal runs were performed on wet sample blends wood-SS (50:50, 30 mg) from 40 °C to the desired curing temperatures of 60 or 105 °C at 20 °C /min and held isothermally for 24 h. Temperature ramp scans were done on wet and cured sample blends (4–6 mg) from 40 to 900 °C at 20 °C/min. Data was analyzed using the Pyris v13.3.1 software.

2.5 Rheology

Curing and flow behavior of wet wood-SS molded discs (2.00 mm (h) x 25 mm (Ø)) was determined from dynamic rheology measurements (complex viscosity (η*), storage modulus (G'), and Tan δ) performed on a Discovery Hybrid Rheometer (DHR2, TA instruments, New Caste, DE, USA) between two serrated parallel plates. For SS curing experiments, flat parallel plates (25 mm Ø) were used. Temperature ramp experiments were from 30 to 200 °C at 2 °C/min with 0.1% strain and frequency of 1 Hz. Frequency sweep experiments were performed isothermally at 22 °C using a Peltier plate with a 0.1% strain from 0.01 to 100 Hz to obtain lower shear rate flow property values with controlled sample temperature. Results were analyzed using the TRIOS software v5.1.1.

Capillary rheology experiments were performed using two capillary rheometers to determine the flow curves of the wet wood-SS blends at higher shear rates. Experiments were performed at room temperature (22 °C) using an Instron 5500R-1137 universal testing machine at crosshead speeds 2, 6, 10, 20, 60, and 100 mm/min. The small capillary rheometer (Instron model 3213) was originally used with a barrel diameter of 9.55 mm, two dies of different lengths (14 and 55 mm) and diameter of 4.0 mm equipped with a 44 kN load cell. To produce larger diameter rods a larger custom-built capillary rheometer was used with a barrel diameter of 44.45 mm, a die length of 19.05 mm, and die diameter of 8.89 mm. It was equipped with a 133 kN load cell (Figure S4). Data were acquired and analyzed using the Bluehill v3 Instron software according to the ASTM D3835-02 standard. Rheological data were also fitted to the Ostwald's power law model of Eq. 1.

$$\sigma = K\gamma^n \tag{1}$$

where σ is the shear stress, γ is the shear rate, K is the consistency index and n is the flow behavior index which is dimensionless (Yoo and Yoo 2005; Lewandowski et al. 2016).

2.6 Extrusion system

An extruder was custom-built to extrude wood-SS mixtures (Figure S3 in Supplemenatry Information). The screw (5 mm pitch) and barrel, with a 35 mm Ø barrel and 420 mm length, were provided by RobotDigg (Shanghai, China). A mild steel 13.5 mm Ø die was secured to the end of the extruder barrel. The screw was coupled to a geared motor (745.7 W, 0–40 RPM, NORD, USA) with a variable frequency drive (Altivar 12). Blends of wood-SS (200 g) were manually fed into the extruder and run for 3 min, with slow screw speeds 0–20 rpm and high screw speeds 21–40 rpm to produce extruded rods.

2.7 Curing extruded rods

The wet extruded rods were cured separately using five different temperature regimes which includes 11 d at 22 °C, 2 d at either 45 °C, 50 or 60 °C, and at two different temperatures (1 d at 60 °C and then 1 d at 105 °C). The wood-SS (60:40) sample rods were only cured for 2 d at 50 °C.

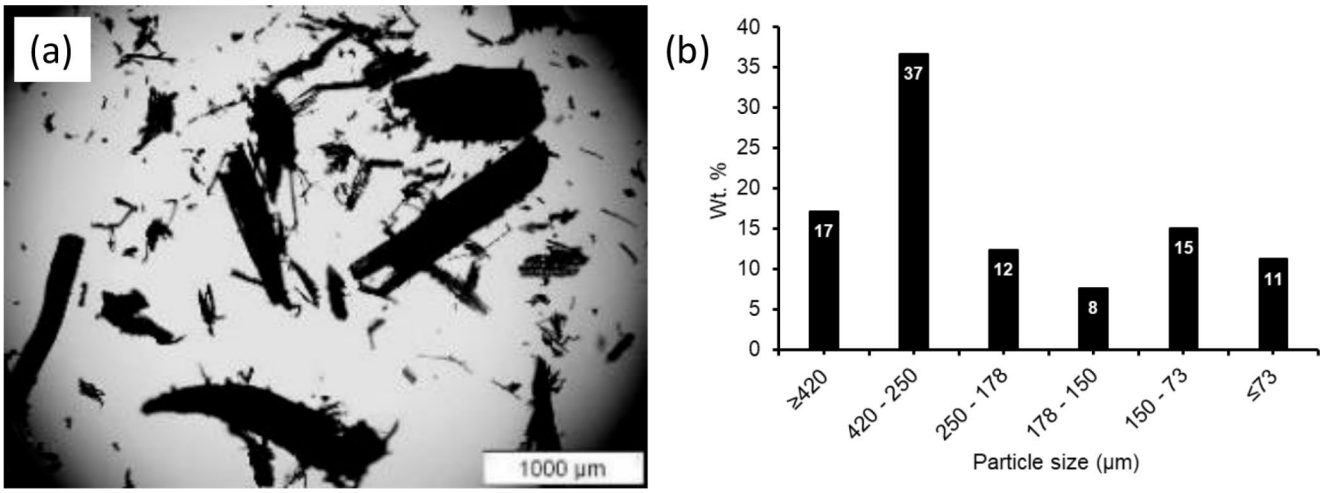

Fig. 1 (a) Optical micrograph (40x) of screened 40 mesh wood fiber and (b) size distribution curve from sieve analysis done on the screened 40 mesh wood fiber

Density was determined on wet and cured samples using the mass per unit volume method.

2.8 Flexural, water soak, and fire tests

Flexural three-point bending tests were performed on cured extruded rod specimens (13.5 mm Ø x 240 mm, 5 replicates) according to ASTM D790, using a Mecmesin MultiTest-dV 2.5 test machine (Virginia, USA), using a 2.5 kN load cell, support span of 216 mm and crosshead speed of 5 mm/min. Data were acquired and analyzed using the Vector Pro v6.11 software. Data were statistically tested using single factor ANOVA using Excel (Microsoft Office 2017) with a 95% confidence interval.

Dimensional stability of the various cured extruded wood-SS rods (2 mm x 13.5 mm Ø) was determined after soaking in water for 24 h at 22°C according to ASTM D570. Percent weight gain and thickness swell were determined based on original and soaked dimensions.

A simple Bunsen burner fire test was performed on wood-SS (50:50) cured composites, in triplicate, for smoldering and flame retardancy. Samples were exposed to the tip of the Bunsen burner flame (1000–1100 °C) and monitored for 5 min via a thermocouple and video camera. Images taken from the video were analyzed every minute for sample changes and final weight loss recorded.

3 Results and discussion

3.1 Fiber characterization

The screened wood fiber had a moisture content of 5.2%. Wood fiber dimensions (width and length) were determined by optical microscopy (Fig. 1a) in conjunction with image analysis. Sieve analysis plot for 40-mesh screened wood fibers is shown in Fig. 1b. The fiber length ranged from 18 to 1929 µm with a mean of 206 ± 242 µm. The fiber width ranged from 12 to 1716 µm with a mean of 192 ± 227 µm. The average aspect ratio of the fibers was 1.3. Longer fibers passed through the mesh screens vertically hence the length was larger than the screen holes. Sieve analysis of the fibers (Fig. 2b) shows the 40 – 20 mesh (250–420 µm) fraction was 37 w/w% while the size range 60–200 mesh (73–250 µm) contained 46 w/w%. 17 w/w% of fibers was > 40 mesh (> 420 µm). Sieve analysis supports the presence of long fibers as observed by image analysis.

3.2 Blending of wood-SS and rheology of wet mixtures

Wood-SS wet samples were freshly mixed and homogenized for each experiment to minimize drying and curing reactions from occurring prior to analysis. To understand the flow properties and steady shear rheological behavior, dynamic rheology frequency sweep and capillary rheology experiments were performed on wood-SS and SS samples.

Frequency sweep experiments at 22°C were done to determine the influence of shear rate (Hz) on the elastic (G′) and loss (G″) moduli of SS and wood-SS wet blends as seen in Fig. 2a. G′ and G″ both increased with an increase in shear rate and generally G′ > G″ showing more elastic behavior. The lower G″ was associated with the molecular friction and loss of energy in the viscous material (Artner et al. 2021). A rapid increase in G′ was observed for SS due to the viscoelastic nature of the material (Sandomierski et al. 2020). Cross over points, where G′ = G″, is assigned to the gel point which did not occur for the wood-SS blends,

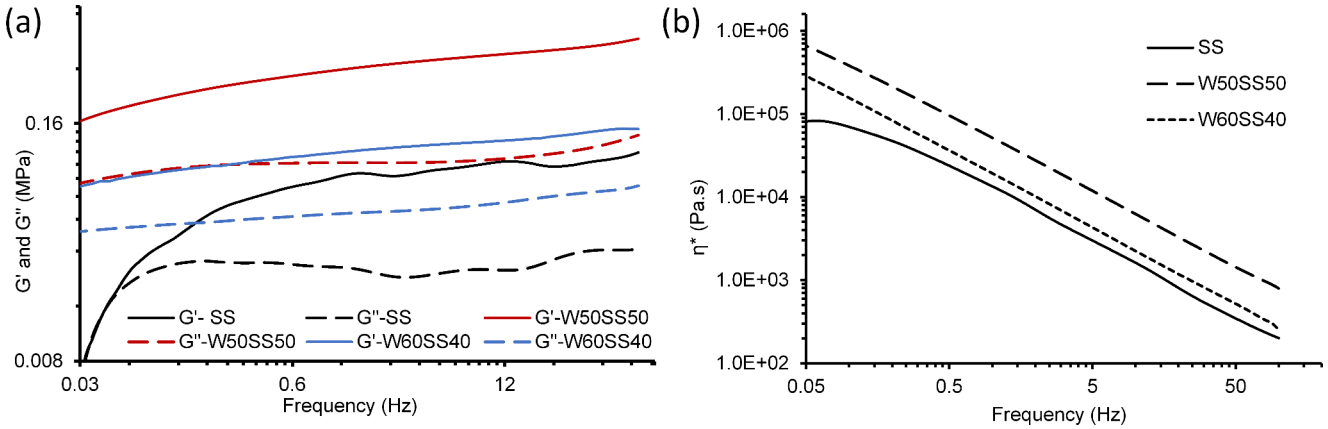

Fig. 2 (a) Elastic (G') and viscous (G") moduli versus frequency plots of SS and wood-SS blends and (b) flow curves (η* vs. frequency) for SS and wood-SS blends

Table 1 Dynamic viscosity values at 1 Hz and flow behavior index (*n*) and consistency coefficient (K)

Sample	η* at 1 Hz (kPa.s)	K (kPa.s)	*n*	R^2 values
SS	13	11	0.83	0.8191
wood-SS (50:50)	52	47	0.87	0.9604
wood-SS (60:40)	19	18	0.91	0.9575

however, for SS a cross-over frequency of 0.04 Hz was observed. With an addition of 50% wood, the stiffness of the matrix increases and the G' increases showing a solid-like elastic behavior and increased dense network. The reduction in the SS content from 50 to 40% in the presence of wood resulted in the reduced molecular interactions between the SS chains which leads to the reduction in the G' (Berlangieri et al. 2018). This resulted in a 65% decrease in G′ at 1 Hz.

Flow curves (complex viscosity (η*) vs. shear rate) for wet wood-SS blends are shown in Fig. 2b and η* values at 1 Hz are documented in Table 1. Shear thinning behavior of SS and wood-SS blends was observed for all samples (Zhu et al. 2017). In contrast, Yang et al. (2008) had shown a shear thickening behavior for SS solutions from 17 to 34% concentrations. The η* of SS at 1 Hz was 13 kPa.s and increased by 286% upon addition of 50% wood fibers. Adding more wood fiber to 60% reduced the η*. This finding was in contrast to previous studies which have shown an increase in viscosity with wood content in wood plastic composites systems (Kaseem et al. 2017; Laufer et al. 2017; Li and Wolcott 2004; Duretek et al. 2015; Mazzanti and Mollica 2020).

The flow curves for wood-SS blends (0.05–100 Hz) generally followed a power law fit model. However, for SS showed a deviation at low frequency and the power law model was thus fitted between 0.1 Hz and 100 Hz.". The power law parameters fitted well with coefficient R^2 values (Table 1) of 0.82 for SS and ~ 0.96 for SS-wood blends. The tendency for the viscosity to change with shear rate can be explained with the flow behavior index (*n*) (Lewandowski et al. 2016). The samples have *n* values between 0.83 and 0.91 indicative of a pseudoplastic material (Pongsawatmanit et al. 2006). The *n* value increased with the addition of wood fiber to SS and increased fiber content from 50 to 60%. In contrast to this, Feng et al. (2011) recorded a reduction in *n* values with increased fiber content due to stronger shear thinning behavior in the study of sisal fiber and poly-butylene-succinate composites. Manning et al. (2019) stated that there was a decrease in *n* values with increased addition of a polyether amine and a nano-clay filler causing a decrease in the shear thinning behavior. The magnitude of K increased with the addition of wood fiber to the SS and reduced with increased wood composition from 50 to 60% (Lewandowski et al. 2016; Li et al. 2020).

Capillary rheology (in the small system) was used to study the extrudability of the wood-SS (50:50) blends at high shear rates (γ) comparable to extrusion using two die lengths at room temperature (20–23 °C). Images of the extrudates for the small and large capillary rheometer are shown in Fig. 3a. Bagley and Rabinowitch corrections were performed on the rheological results according to ASTM D3835 to obtain true viscosity (η_{true}) and γ values (Fig. 3b; Table 2). The γ obtained were between 2 and 100 s^{-1}. The η_{true} decreased with γ and values obtained were from 49.4 to 1.2 kPa.s (Table 2). Shear thinning and pseudoplastic behavior was also observed with an increase in shear rate as seen with most polymer melts (Lewandowski et al. 2016). The flow curve followed a power-law fit model and the model parameters (*n* and K) are given in Table 2. The power law component, *n* for the wood-SS (50:50) decreased to 0.76 and consistency coefficient value, K, increased to 92 kPa.s in comparison to the dynamic rheology results showing a higher shear thinning behavior at higher shear rates (Mazzanti and Mollica 2020).

Table 2 Viscosity values for small and large capillary rheology dies

Shear rate (1/s)	η_{true} (kPa.s)	*n* values	K values (kPa.s)	R^2
Small capillary rheology				
2.0	49.4	0.76	92	0.998
6.0	15.7			
10.0	10.5			
20.1	5.8			
60.2	1.9			
100.3	1.2			
Large capillary rheology				
1.4	225.0	0.95	339	0.979
4.1	123.1			
6.9	90.1			
13.8	52.2			
41.4	19.4			
68.9	12.4			

A large capillary rheometer was constructed to produce large diameter rods for evaluation. The large capillary rheometer had a single die length and η was calculated with an intercept pressure value considered as zero. Values for γ were from 1.4 s^{-1} to 69 s^{-1} and with a concomitant shear η from 225 to 12.4 kPa.s (Table 2). The η values from the small capillary rheometer were lower than those obtained with the larger system. Values from the larger capillary rheometer were not corrected for true shear stress according to Bagley since only one die length was used (ASTM D3835) hence the higher range of η_{true} values. Bagley corrections are essential to account for pressure losses sustained by the sample in motion from the barrel to the capillary die, die entrance and effects with different die lengths (Mazzanti and Mollica 2020). The flow curves also followed a power-law fitted model (Table 2; Fig. 3b). A 25% increase was observed for the power law index *n* in the large capillary rheometer and K values increased over 200%. The rheological measurements on the wood-SS (50:50) blend from the dynamic, and two capillary rheometers are shown together in Fig. 3b. In comparison to the dynamic rheology, the capillary rheology true viscosity values are slightly higher due to the influence of the pressure driven methodology and increased shear rate which causes the increase in viscosity values (Mazzanti anf Mollica 2020). All flow curve plots (dynamic and capillary) had similar slopes, but a definite offset (K) was observed.

3.3 Curing of wood-SS blends (DSC, Isothermal TGA and temp ramp rheology)

The curing of SS and wood-SS blends was monitored by DSC. To improve the resolution of the analysis of these wet materials, modulated DSC (MDSC) was used to obtain the reversible and non-reversible heat flow and heat capacity data. Curing reactions were observed by the presence of exothermic peaks in the DSC thermograms of SS and wood-SS blends (Fig. 4a). The peak temperature and enthalpy of SS and wood-SS blends are given in Table 3. To verify these exotherms, MDSC curves of the wood particles were obtained (Fig. 4b), and exothermic peaks were not seen except between 45 and 60 °C. The area under each

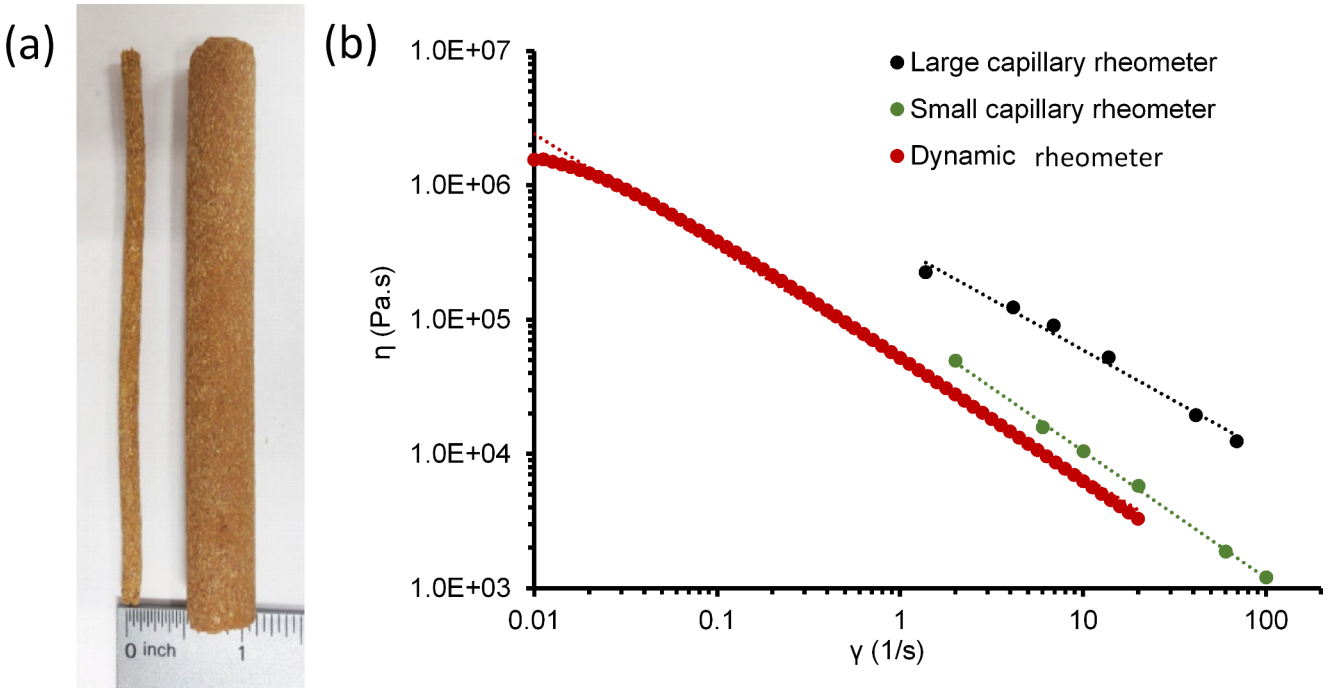

Fig. 3 (a) Photograph of extrudates from the small and large capillary rheometer and (b) viscosity versus shear rate (flow curves) plots of wood-SS (50:50) blend by dynamic and capillary rheometry at 22 °C

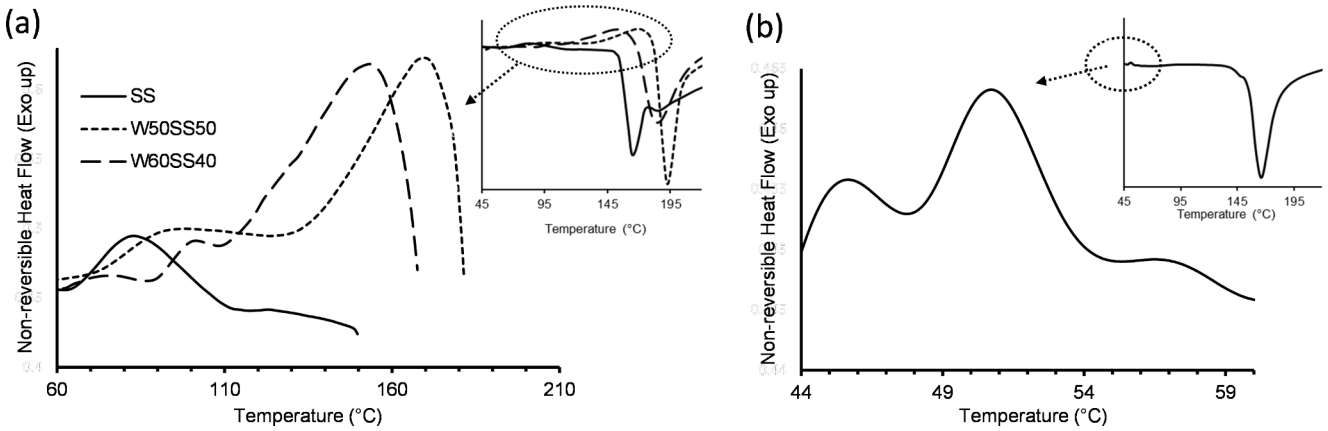

Fig. 4 (a) Nonreversible heat MDSC heat flow thermograms of SS and wood-SS blends and (b) MDSC heat flow thermograms of wood fiber

Table 3 MDSC peak values for wood and SS samples

Sample	Major Exothermic Peak (°C)	Enthalpy (J/g)
SS	83 (±0.6)	6.4 (±0.5)
Wood-SS (50:50)	163 (±9.2)	23.2 (±8.2)
Wood-SS (60:40)	153 (±2.0)	31.5 (±6.9)

curve was measured for the enthalpic heat of reaction. Kelley et al. (1987) in a study of spruce wood attributed the DSC peak at 50 °C to enthalpy relaxation which is closely associated with the glass transition temperature (T_g) (Kelley et al. 1987). The enthalpy of curing and the intensity of exotherms also increased with the addition of wood. It is assumed that with an increase in wood content, the curing of SS occurred at a lower temperature due to the free movement of SS molecular chains (Phiri et al., 2020). Major curing peak temperatures were seen at 83 °C, 163 °C and 153 °C for SS, Wood-SS blends at 50:50 and 60:40, respectively. Zhou et al. (2009) observed two endothermic peaks for SS at 88.3 and 126.1 °C for the dehydration condensation of the silanol groups in SS and further condensation, respectively).

The curing behavior of SS and wood-SS blends was also examined by dynamic rheology (η^* and tan δ) using a temperature ramp (Fig. 5). This approach was used by Katoueizaha et al. (2020) and Pham and Hatzignatiou (2016) to investigate the gelation of SS. At low temperature (30–50 °C), the curing reaction is slow and a slight increase in η^* was observed. As the temperature increases from 50 to 105 °C, the η^* decreases due to softening of SS. Finally, > 105 °C there was a rapid rise in η^* as the SS goes from a liquid to a gel and then to a vitrified glass (Candan et al. 2016). During the curing of SS, foaming and spreading of the solution occurred with an increase in temperature leaving a foam-like residue. Subasri and Näfe (2008) recorded that this foaming reaction occurs between 400 and 750 °C for pure SS followed by the crumbling of the structure. The sharp increase in η^* of SS shows the start of gelation under the low strain used. With the addition of wood fibers to SS, the mixture has a higher η^* (Domínguez 2018; Vasconcelos et al. 2021). For the wood-SS blends, the temperature at maximum η^* was 110 °C for 50:50 mix and 103 °C for 60:40 mix were assigned to gelation. The max η^* for the wood-SS 50:50 blend was higher than the 60:40 blend and could be attributable to a decrease in SS content.

Tan δ (G″/G′) plot against temperature (Fig. 5b) was used to establish gelation of the SS. Tan δ for the formulations is dependent on fiber volume fraction, temperature and type of fibers (Vasconcelos et al. 2021). As temperature increased tan δ increased to a maximum (104 °C for SS, 108 °C for 50:50 blends and 96 °C for 60:40 blend) which corresponded to more molecular mobility (liquid behavior). Tan δ then decreased to a minimum with temperature (120 °C for 60:40 blend and 135 °C for 50:50 blend) and this was assigned to the gelation point. Tan δ was highly influenced by wood content (fiber fraction) which can restrict polymer chain movement (Phiri et al., 2020; Joseph et al. 2010).

The curing behavior of wood-SS 50:50 blend was also studied by isothermal TGA by examining temporal loss in weight of water (Fig. 6). The thermogram curves show a weight loss of 37% at 10 min while being cured at 105 °C. While at 60 °C curing took 24 min to achieve a 37% weight loss. The final weight loss after 24 h of isothermal curing at 60 and 105 °C was about 40–41%.

3.4 Extrusion of wood-SS blend

The wood was blended into SS in a 50:50 or 60:40 ratio using high shear mixer and a slight warming of the mix was observed which was attributed to an exothermic reaction of SS reacting with ambient CO_2, which was about 400 ppm (Brown 2000; Lüthi et al. 2008). The mixture was fed into the extruder and the screw speed was shown to greatly influence the surface smoothness (< 20 rpm) or roughness (Fig. 7). At higher screw speed 21–40 rpm, shark skin

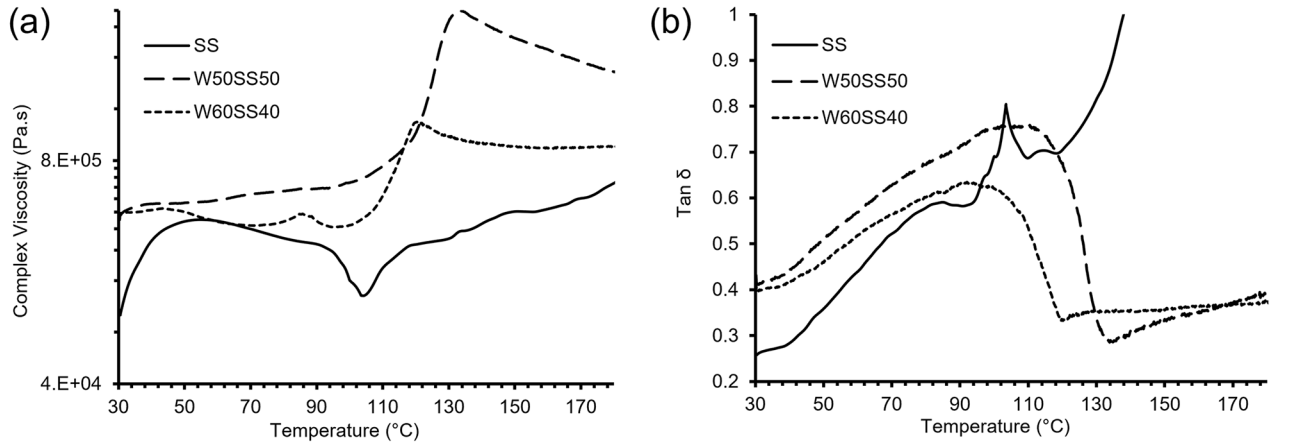

Fig. 5 (a) Complex viscosity (η*) plots against temperature and (b) Tan δ plots against temperature for SS and wood-SS blends

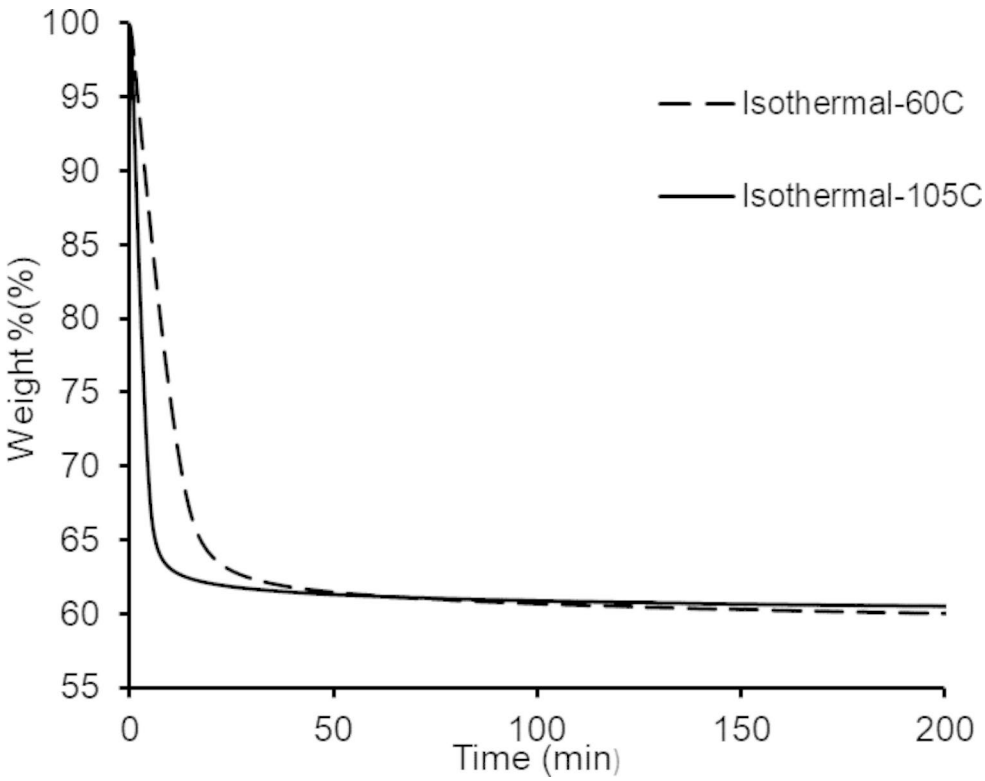

Fig. 6 Isothermal TGA thermograms for wood-SS 50:50 blend at 60 and 105 °C

(surface fracture) was observed in the extruded rod due to elastic surface instability (Venet and Vergnes 2000). Several arguments have also attributed this occurrence to some stick-slip phenomena which occur at the die-exit (Vlachopoulos and Strutt 2003).

The extruded rods were initially cured at 105 °C and surface cracks were formed and possibly due to differential stresses caused by a moisture gradient. Therefore, different curing regimes (22, 45, 50, 60 and 105 °C at different times) were explored to mitigate crack formation. Crack formation can be attributed to the rapid shrinkage of the composite surface, at higher temperature, whilst loosing water due to thermal stresses (Kodur et al. 2016).

The density of the wet extruded rods ranged between 0.96 and 1.42 g/cm^3 (Table 4). The density of the rods decreased after curing to between 0.79 and 0.92 g/cm^3. This decrease in density resulted from water removal (Gul et al. 2017; Bilgin Guller 2012).

The chemical features of wood fiber and SS blends were determined by FTIR spectroscopy (Fig. 8). The main absorption bands for SS were seen between 500 and 1200 cm^{-1} and assigned to vibrations of the silicate group (Izak et al. 2018; Rao et al. 2007; Cheng 2013). The distinct

Fig. 7 Photographs of (a) smooth extruded wood-SS (50:50) rods and (b) extruded wood-SS showing sharkskin

Table 4 Wet and cured density calculations for extruded wood-SS 50:50 and 60:40 blends

Sample	Curing time (d = days) and temperature	Wet Density (g/cm^3)	Cured Density (g/cm^3)
Wood-SS (50:50)	11 d at 22 °C	1.42 (± 0.02)	0.92 (± 0.02)
	2 d at 45 °C	1.34 (± 0.02)	0.86 (± 0.02)
	2 d at 50 °C	1.33 (± 0.02)	0.83 (± 0.02)
	2 d at 60 °C	1.33 (± 0.04)	0.79 (± 0.03)
	1 d at 60 °C + 1 d at 105 °C	0.96 (± 0.03)	0.84 (± 0.02)
Wood-SS (60:40)	2 d at 50 °C	1.30 (± 0.05)	0.89 (± 0.05)

Note: Standard deviation in parentheses

band at 1001 cm^{-1}, which has two shoulders was attributed to the Si-O-Si stretching vibrations. This band is known to shift to higher frequency with an increase in the degree of polymerization of silicate ions in SS (Izak et al. 2018). The two shoulders at 888 cm^{-1} and 1100 cm^{-1} were assigned to Si-OH bonds (Rao et al. 2007; Cheng 2013). The bands at 3364 cm^{-1} and 1639 cm^{-1} were due to the presence of water and O-H stretching modes. The low intensity bands between 2100 cm^{-1} and 2400 cm^{-1} were assigned to hydrogen bridging in the silicate lattice (Koohestani et al. 2021; Bobrowski et al. 2012; Firdous et al. 2021)

The wood fiber spectrum (Fig. 8) showed an intense O-H stretching band at 3329 cm^{-1}. A C-H stretching band at 2880 cm^{-1} was also observed and assigned to wood polymers and extractives (Sayılkan et al., 2004). The band at ~ 1100 cm^{-1} was assigned to C-O stretching of cellulosic polysaccharides. Bands at 1507 cm^{-1} and 1600 cm^{-1} were assigned to lignin aromatic units (Cheng et al. 2016). The band at 1730 cm^{-1} was assigned to an ester carbonyl (C = O) groups in hemicellulose (Pandey 1999; Pillai et al. 2011).

FTIR spectroscopy was employed to examine the chemistry of the cured wood-SS material performed at different curing regimes (Fig. 8). The wet wood-SS mixture showed a large O-H stretching band at 3334 cm^{-1} and 1639 cm^{-1} due to the presence of water (Bobrowski et al. 2012). In addition, the mix had bands associated with wood and SS, as described above. Upon curing of the wood-SS mix the O-H stretching band (centered at 3300 cm^{-1}) decreased in intensity and was temperature dependent. This decrease was attributed to the removal of hydroxyl groups, dehydration and crosslinking reactions that occurred (Le and Le 2021).

During curing the C-H stretching (methylene) bands at 2800 cm^{-1} and 3000 cm^{-1} became visible. The Si-O-Si, C-O stretching and Si-O symmetric stretching bands centered at 1000 cm^{-1} also increased in intensity (Chen et al. 2014; Sayılkan et al. 2004; Ukaji et al. 2007). Si-O-C vibrations were also seen at 1260–1270 cm^{-1} for all cured samples (Valadez-Gonzalez et al. 1999). The lignin aromatic units in wood were also detected at 1508 and 1600 cm^{-1}. The skeletal C-C band centered at 1420 cm^{-1} was shown to increase in intensity with curing temperature. In addition, the carbonyl band around 1700 cm^{-1} associated with hemicellulose was also observed (Cheng et al. 2016; Wang et al. 2016). These results show that FTIR spectroscopy clearly found chemical functional group differences between wood-SS blends cured at different temperatures.

3.5 Flexural, thermal degradation, water soak and fire properties

The flexural strength and modulus of the extruded wood-SS (50:50 and 60:40) cured rods were determined and the results are given in Table 5. The flexural stress of the 50:50 blend rods cured between 22 and 60 °C was about 24 MPa and not significant. The strength significantly decreased to 11 MPa for wood-SS cured using the 2-step regime (60 °C plus 105 °C). Lower values of flexural strength in pine, SS and clay composites were observed when cured at 75 °C (Berzins et al. 2017). The decrease in strength may be attributable to (i) non-homogenous cross-linked structures (Gupta et al. 1985) and/or (ii) the formation of voids in the matrix due to water formed bubbles as evident from its low wet density (Tang et al. 2017). Changing the wood-SS blend ratio from 50:50 to 60:40 (cured at 50 °C) did not significantly change the flexural strength of the composite.

The flexural modulus of the 50:50 blend rods cured between 22 and 60 °C was about 4.5 GPa and was not significantly different (Table 5). The modulus decreased significantly by half when the wood-SS mix was cured at higher temperature. By increasing the wood content from 50 to 60% (cured at 50 °C) there was no significant change in flexural modulus.

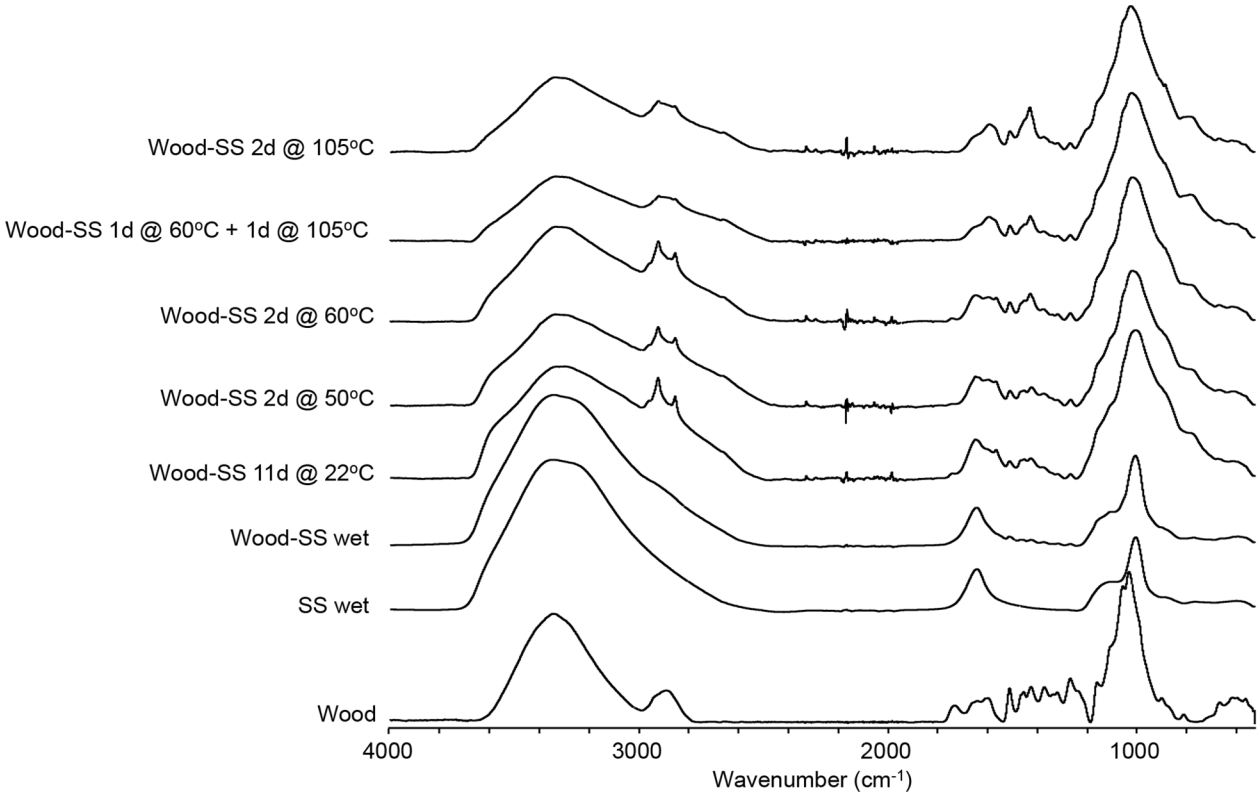

Fig. 8 FTIR spectra of wood fiber, SS solution, wood-SS (50:50) wet mix, and wood-SS (50:50) cured at different times and temperatures

Table 5 Bending strength values for wood-SS (50:50 and 60:40) extruded samples cured at different temperatures

Cured wood-SS sample	Flexural Stress (MPa)	Modulus of Elasticity (GPa)
50:50 blend		
11d at 22 °C	23.5 (±1.5)[a]	4.3 (±0.2)[b]
2d at 45 °C	23.9 (±2.0)[a]	4.6 (±0.2)[b]
2d at 50 °C	24.7 (±2.2)[a]	4.6 (±0.4)[b]
2d at 60 °C	23.2 (±3.7)[a]	4.4 (±0.6)[b]
1d at 60 °C + 1d at 105 °C	11.1 (±1.1)[b]	2.3 (±0.2)[a]
60:40 blend		
2d at 50ºC	25.0 (±2.0)[a]	4.3 (±0.6)[b]

Note: Standard deviation in parentheses. Samples with different superscript letters (a, b, c) are statistically different ($p < 0.05$) using a single factor ANOVA test

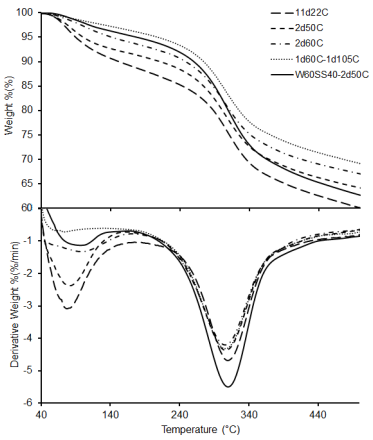

Fig. 9 TGA and DTG thermograms of wood-SS samples cured at different temperatures

The thermal stability of the cured wood-SS materials and the effect of increased wood composition in the blends was studied by TGA. Thermograms and TGA values are seen in Fig. 9; Table 6, respectively. The wood-SS (50:50) sample cured for 11 d at 22 °C had the lowest residual weight of 57% (Fig. 9). As the curing temperature increased the higher the residual weight remained (65% at 60 °C + 105 °C). The weight loss of the cured wood-SS occurred in 2 stages, as observed by two negative DTG peaks, between 40–140 °C and 140–440 °C. Water loss occurred between 40–140 °C (Sarmin et al. 2014; Zuhua et al. 2009; Tran et al. 2019). The intensity of the water loss DTG peaks is seen to reduce with increased curing temperature. Li et al. (2013) reported a similar range of degradation temperature for SS from 75 to 221 °C associated with water loss. The second degradation

Table 6 Thermogram peak values for the cured wood-SS composites

Curing time and temperature	First Peak (°C)	Second Peak (°C)	Residual (%)
50:50 blend			
11 d at 22 °C	79 (±4.5)	310 (±2.3)	57 (±1.1)
2 d at 45 °C	76 (±2.1)	305 (±1.1)	57 (±1.4)
2 d at 50 °C	77 (±3.7)	307 (±1.2)	61 (±0.5)
2 d at 60 °C	103 (±6.2)	305 (±2.4)	63 (±0.5)
1 d at 60 °C + 1 d at 105 °C	-	307 (±1.9)	65 (±0.7)
60:40 blend			
2 d at 50 °C	77 (±5.3)	309 (±2.6)	55 (±3.0)

Note: Standard deviation in parentheses

stage is associated with the breakdown of silanol groups and wood components (Li et al. 2020; Zaharescu et al. 2018)

With an increase in wood content to 60%, a lower residual weight was recorded at 55% in comparison to 61% for wood-SS (50:50) samples, which were cured at 50 °C. This is due to the presence of unbonded wood particles and low thermal stability of the lignocellulosic components in wood fiber. Natural fillers like wood in increased amounts are known to reduce the thermal stability of composites hence the observed residual weight reduction (Nabinejad et al. 2017).

3.6 Water absorption properties

The wood-SS composites were evaluated for their water resistance by performing a 24 h water soak test. All the wood-SS composites cured between 22 and 60 °C disintegrated after 24 h water soaking. The wood-SS sample cured at the higher temperature (1 d at 60 °C + 1 d at 105 °C) remained intact after water soaking (80% weight gain and 21% thickness swell). It appears that curing at low temperature removed the water from the wood-SS mix but did not cross-link the SS and that the higher curing temperature resulted in SS crosslinking (Sarmin, 2016) .

3.7 Fire test

The wood-SS (50:50) composite cured at the higher temperature was evaluated for its fire resistance using a Bunsen burner test over 5 min (Fig. 10). At 1 min the composite bent slightly. After 5 min the sample exhibited no smoldering once the flame was removed and an average weight loss of 20% was recorded. Visual inspection of the flame-tested sample (Fig. 10d) showed some small sub-mm diameter perforations (holes) on the surface with a physically intact structure showing the wood-SS composite's qualitatively fire resistant properties.

4 Conclusion

Composites made from wood-SS were successfully blended, extruded into 2-dimensional rods, and cured. The wood-SS blends were shown to have good rheological properties suitable for extrusion and additive manufacturing. Wood-SS (50:50) samples exhibited good thermal stability, burning properties and flexural properties. The flexural properties decreased with higher curing temperatures. The water soak performance of the low temperature cured composites was not satisfactory; however, at higher temperature curing the composites performed well. The wood-SS composite material shows potential for use in additive manufacturing for interior applications. Furthermore, SS is an inexpensive non-toxic binder in fire resistant natural fiber composites. To move this technology forward further work is required to (i) fully understand the curing mechanism of SS in wood blends, (ii) improve the curing process to have good water performance as well as flexural properties, (iii) integrate the extruder into a 3D printer, and (iv) study interlayer bonding.

Acknowledgements The authors would like to acknowledge (i) the Idaho State Board of Education-Higher Education Research Council-IGEM award # IGEM 20 – 002 for their financial support, (ii) USDA-CSREES grant 2007-34158-17640 for support in the purchase of the DSC, and the University of Idaho College of Natural Resources for support in the purchase of the FTIR spectrometer.

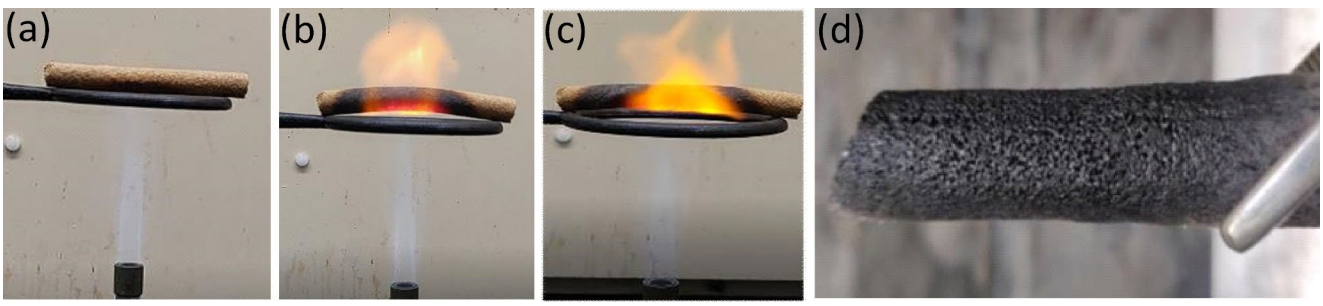

Fig. 10 Photographs of the wood-SS (50:50) composite during a Bunsen burner flame test at (a) 0 min, (b) 2 min, (c) 4 min, and (d) after 5 min (test completed)

Declarations

Conflict of interest On behalf of all authors, the corresponding author states that there is no conflict of interest.

References

Additive Manufacturing Materials Market – Industry Reports. https://www.industryresearch.co/additive-manufacturing-materials-market-13999766

Antov P, Savov V, Neykov N (2020) Sustainable bio-based adhesives for eco-friendly wood composites. A review. WOOD Res 65:15. https://doi.org/10.37763/wr.1336-4561/65.1.051062

Artner MA, de Cademartori PHG, Avelino F, Lomonaco D, Magalhães WLE (2021) A novel design for nanocellulose reinforced urea–formaldehyde resin: A breakthrough in amino resin synthesis and biocomposite manufacturing. Cellulose 28(6):3435–3450. https://doi.org/10.1007/s10570-021-03739-4

Bagheri A, Jin J (2019) Photopolymerization in 3D Printing. ACS Appl Polym Mater 1(4):593–611. https://doi.org/10.1021/acsapm.8b00165

Berlangieri C, Poggi G, Murgia S, Monduzzi M, Baglioni P, Dei L, Carretti E (2018) Structural, rheological and dynamics insights of hydroxypropyl guar gel-like systems. *Colloids and Surfaces B: Biointerfaces*, *168*. https://doi.org/10.1016/j.colsurfb.2018.02.025

Berzins A, Morozovs A, Gross U, Iejavs J (2017) *Mechanical properties of wood-geopolymer composite*. 1167–1173. https://doi.org/10.22616/ERDev2017.16.N251

Bifulco A, Silvestri B, Passaro J, Boccarusso L, Roviello V, Branda F, Durante M (2020) A New Strategy to Produce Hemp Fibers through a Waterglass-Based Ecofriendly Process. Materials 13(8):1844. https://doi.org/10.3390/ma13081844

Bilgin Guller (2012) Effects of heat treatment on density, dimensional stability and color of Pinus nigra wood. Afr J Biotechnol 11(9):2204–2209. https://doi.org/10.5897/AJB11.3052

Bobrowski A, Hutera BStypuła, Kmita B, Drożyński A, Starowicz D, M (2012) FTIR spectroscopy of water glass—The binder moulding modified by ZnO nanoparticles. Metalurgija -Sisak Then Zagreb 4:477–480

Brown JR (2000) Sodium silicate bonded sand. In *Foseco Ferrous Foundryman's Handbook* (pp. 204–215). Elsevier. https://doi.org/10.1016/B978-075064284-2/50015-6

Buschmann B, Henke K, Talke D, Saile B, Asshoff C, Bunzel F (2021) Additive Manufacturing of Wood Composite Panels for Individual Layer Fabrication (ILF). Polymers 13(19):3423. https://doi.org/10.3390/polym13193423

Candan Z, Gardner DJ, Shaler SM (2016) Dynamic mechanical thermal analysis (DMTA) of cellulose nanofibril/nanoclay/pMDI nanocomposites. Compos Part B: Eng 90:126–132. https://doi.org/10.1016/j.compositesb.2015.12.016

Chai W, Zhang L, Li W, Zhang M, Huang J, Zhang W (2021) Preparation of Plastics- and Foaming Agent-Free and Porous Bamboo Charcoal based Composites Using Sodium Silicate as Adhesives. Materials 14(10):2468. https://doi.org/10.3390/ma14102468

Chen H, Lang Q, Bi Z, Miao X, Li Y, Pu J (2014) Impregnation of poplar wood (Populus euramericana) with methylolurea and sodium silicate sol and induction of in-situ gel polymerization by heating. Holzforschung 68(1):45–52. https://doi.org/10.1515/hf-2013-0028

Chen Q, Zhang R, Qin D, Feng Z, Wang Y (2018) Modification of the Physical-mechanical Properties of Bamboo-plastic Composites with Bamboo Charcoal after Hydrothermal Aging. BioResources 13(1):1661–1677. https://doi.org/10.15376/biores.13.1.1661-1677

Cheng S, Huang A, Wang S, Zhang Q (2016) Effect of Different Heat Treatment Temperatures on the Chemical Composition and Structure of Chinese Fir Wood. BioResources 11:4006–4016. https://doi.org/10.15376/biores.11.2.4006-4016

Cheng X (2013) Superhydrophobic sodium silicate based silica aerogel prepared by ambient pressure drying. *Materials Chemistry and Physics*, *141(1):570–575*. https://doi.org/10.1016/j.matchemphys.2013.05.064

Cherkasova NG (2020) How Adding Wood Dust Affects the Properties of Composite Construction Materials. *IOP Conference Series: Earth and Environmental Science*, *459*, 032054. https://doi.org/10.1088/1755-1315/459/3/032054

Dimas D, Giannopoulou I, Panias D (2009) Polymerization in sodium silicate solutions: A fundamental process in geopolymerization technology. J Mater Sci 44(14):3719–3730. https://doi.org/10.1007/s10853-009-3497-5

Domínguez JC (2018) Chapter 4—Rheology and curing process of thermosets. In Q. Guo (Ed.), *Thermosets (Second Edition)* (pp. 115–146). Elsevier. https://doi.org/10.1016/B978-0-08-101021-1.00004-6

Duretek I, Schuschnigg S, Gooneie A, Langecker GR, Holzer C (2015) *Rheological properties of wood polymer composites and their role in extrusion*. Journal of Physics: Conference Series, *602*, 012014. https://doi.org/10.1088/1742-6596/602/1/012014

Falk B, McKeever D (2012) *Generation and Recovery of Solid Wood Waste in the U.S.* BioCycle August 2012, Vol. 53, No. 8, p. 30

Feng Y-H, Zhang D-W, Qu J-P, He H-Z, Xu B-P (2011) Rheological properties of sisal fiber/poly(butylene succinate) composites. Polym Test 30(1):124–130. https://doi.org/10.1016/j.polymertesting.2010.11.004

Firdous R, Hirsch T, Klimm D, Lothenbach B, Stephan D (2021) Reaction of calcium carbonate minerals in sodium silicate solution and its role in alkali-activated systems. Miner Eng 165:106849. https://doi.org/10.1016/j.mineng.2021.106849

Gul W, Khan A, Shakoor A (2017) Impact of Hot Pressing Temperature on Medium Density Fiberboard (MDF) Performance. *Advances in Materials Science and Engineering*, *2017*, e4056360. https://doi.org/10.1155/2017/4056360

Gupta VB, Drzal LT, Lee CY-C, Rich MJ (1985) The temperature-dependence of some mechanical properties of a cured epoxy resin system. Polym Eng Sci 25(13):812–823. https://doi.org/10.1002/pen.760251305

Izak P, Ogłaza L, Mozgawa W, Mastalska-Popławska J, Stempkowska A (2018) Influence of the type of aqueous sodium silicate on the stabilization and rheology of kaolin clay suspensions. Spectrochim Acta Part A Mol Biomol Spectrosc 196:155–159. https://doi.org/10.1016/j.saa.2018.02.022

Joseph S, Appukuttan SP, Kenny JM, Puglia D, Thomas S, Joseph K (2010) Dynamic mechanical properties of oil palm microfibril-reinforced natural rubber composites. J Appl Polym Sci 117(3):1298–1308. https://doi.org/10.1002/app.30960

Kaseem M, Hamad K, Deri F, Ko YG (2017) Effect of Wood Fibers on the Rheological and Mechanical Properties of Polystyrene/Wood Composites. J Wood Chem Technol 37(4):251–260. https://doi.org/10.1080/02773813.2016.1272127

Katoueizadeh E, Rasouli M, Zebarjad SM (2020) A comprehensive study on the gelation process of silica gels from sodium silicate. J Mater Res Technol 9(5):10157–10165. https://doi.org/10.1016/j.jmrt.2020.07.020

Kelley SS, Rials TG, Glasser WG (1987) Relaxation behaviour of the amorphous components of wood. J Mater Sci 22(2):617–624. https://doi.org/10.1007/BF01160778

Kodur VKR, Bhatt PP, Soroushian P, Arablouei A (2016) Temperature and stress development in ultra-high performance concrete during

curing. Constr Build Mater 122:63–71. https://doi.org/10.1016/j.conbuildmat.2016.06.052
Koohestani B, Mokhtari P, Yilmaz E, Mahdipour F, Darban AK (2021) Geopolymerization mechanism of binder-free mine tailings by sodium silicate. Constr Build Mater 268:121217. https://doi.org/10.1016/j.conbuildmat.2020.121217
Korniejenko K, Frączek E, Pytlak E, Adamski M (2016) Mechanical Properties of Geopolymer Composites Reinforced with Natural Fibers. Procedia Eng 151:388–393. https://doi.org/10.1016/j.proeng.2016.07.395
Krapež Tomec D, Kariž M (2022) Use of Wood in Additive Manufacturing: Review and Future Prospects. Polymers 14(6):1174. https://doi.org/10.3390/polym14061174
Laufer N, Hansmann H, Koch M (2017) *Rheological Characterisation of the Flow Behaviour of Wood Plastic Composites in Consideration of Different Volume Fractions of Wood*. 790:012017. https://doi.org/10.1088/1742-6596/790/1/012017
Le CM, Le T-H (2021) The Study's Chemical Interaction of the Sodium Silicate Solution with Extender Pigments to Investigate High Heat Resistance Silicate Coating. *Journal of Analytical Methods in Chemistry*, *2021*, e5510193. https://doi.org/10.1155/2021/5510193
Lewandowski K, Piszczek K, Zajchowski S, Mirowski J (2016) Rheological properties of wood polymer composites at high shear rates. Polym Test 51:58–62. https://doi.org/10.1016/j.polymertesting.2016.02.004
Li P, Zhang Y, Zuo Y, Lu J, Yuan G, Wu Y (2020) Preparation and characterization of sodium silicate impregnated Chinese fir wood with high strength, water resistance, flame retardant and smoke suppression. J Mater Res Technol 9(1):1043–1053. https://doi.org/10.1016/j.jmrt.2019.10.035
Li TQ, Wolcott MP (2004) Rheology of HDPE–wood composites. I. Steady state shear and extensional flow. Compos Part A: Appl Sci Manufac 35(3):303–311. https://doi.org/10.1016/j.compositesa.2003.09.009
Li W, Peng J, Guo S, Zhang L, Chen G, Xia H (2013) Carbothermic reduction kinetics of ilmenite concentrates catalyzed by sodium silicate and microwave-absorbing characteristics of reductive products. Chem Ind Chem Eng Q 19(3):423–433. https://doi.org/10.2298/CICEQ120421077L
Lüthi D, Le Floch M, Bereiter B, Blunier T, Barnola J-M, Siegenthaler U, Raynaud D, Jouzel J, Fischer H, Kawamura K, Stocker TF (2008) High-resolution carbon dioxide concentration record 650,000–800,000 years before present. Nature 453(7193):379–382. https://doi.org/10.1038/nature06949
Mamun C, Arifuzzaman M (2020) *Compressive Properties of Sawdust Composites Consisting of Sodium Silicate Solution and Corn Starch as Binder*. 4:129–136. https://doi.org/10.5281/zenodo.3605465
Manning KB, Wyatt N, Hughes L, Cook A, Giron NH, Martinez E, Campbell CG, Celina MC (2019) Self Assembly–Assisted Additive Manufacturing: Direct Ink Write 3D Printing of Epoxy–Amine Thermosets. Macromol Mater Eng 304(3):1800511. https://doi.org/10.1002/mame.201800511
Mazhirin PYu (2002) Influence of Various Factors on the Curing of Sodium-Silicate-Based Composites Cured by Carbon Dioxide. Int Polym Sci Technol 29(3):78–82. https://doi.org/10.1177/030717 4X0202900317
Mazzanti V, Malagutti L, Mollica F (2019) FDM 3D Printing of Polymers Containing Natural Fillers: A Review of their Mechanical Properties. Polymers 11(7):1094. https://doi.org/10.3390/polym11071094
Mazzanti V, Mollica F (2020) A Review of Wood Polymer Composites Rheology and Its Implications for Processing. Polymers 12(10):2304. https://doi.org/10.3390/polym12102304
Ming Y, Duan Y, Wang B, Xiao H, Zhang X (2019) A Novel Route to Fabricate High-Performance 3D Printed Continuous Fiber-Reinforced Thermosetting Polymer Composites. Materials 12(9):1369. https://doi.org/10.3390/ma12091369
Ming-Li L, Chun-Feng L, Yan-Long L (2019) Physical and mechanical properties of modified poplar wood by heat treatment and impregnation of sodium silicate solution. WOOD Res 64:1:145–153
Nabinejad O, Debnath S, Rahman M, Davies I (2017) Effect of filler load on the curing behavior and mechanical and thermal performance of wood flour filled thermoset composites. J Clean Prod 164:1145–1156. https://doi.org/10.1016/j.jclepro.2017.07.036
Ng CW, Yip MW, Lai YC (2018) The Study on the Effects of Sodium Silicate on Particleboard Made from Sugarcane Bagasse. Mater Sci Forum 911:66–70. https://doi.org/10.4028/www.scientific.net/MSF.911.66
Owusu YA (1982) Physical-chemistry study of sodium silicate as a foundry sand binder. Adv Colloid Interface Sci 18(1–2):57–91. https://doi.org/10.1016/0001-8686(82)85031-8
Papadopoulos AN (2020) Advances in Wood Composites. Polymers 12(1):48. https://doi.org/10.3390/polym12010048
Peng Y, Han Y, Gardner DJ (2010) Sodium silicate coated wood. *Proceedings of the International Convention of Society of Wood Science and Technology and United Nations Economic Commission for Europe–Timber Committee (Pp. 11–14). Geneva Switzerland*, 11–14
Pham LT, Hatzignatiou DG (2016) Rheological evaluation of a sodium silicate gel system for water management in mature, naturally-fractured oilfields. J Petrol Sci Eng 138:218–233. https://doi.org/10.1016/j.petrol.2015.11.039
Phiri MJ, Phiri MM, Mpitso K, Hlangothi SP (2020) Curing, thermal and mechanical properties of waste tyre derived reclaimed rubber–wood flour composites. Mater Today Commun 25:101204. https://doi.org/10.1016/j.mtcomm.2020.101204
Pillai K, Mcdonald A, Wagner F (2011) Developing a model system in vitro to understand tracheary element development in Douglas-fir (Pseudostuga mensziesii). Maderas: Ciencia y Tecnología 13:3–18. https://doi.org/10.4067/S0718-221X2011000100001
Pongsawatmanit R, Temsiripong T, Ikeda S, Nishinari K (2006) Influence of tamarind seed xyloglucan on rheological properties and thermal stability of tapioca starch. J Food Eng 77(1):41–50. https://doi.org/10.1016/j.jfoodeng.2005.06.017
Pratheep Kumar S, Takamori S, Araki H, Kuroda S (2015) Flame retardancy of clay–sodium silicate composite coatings on wood for construction purposes. RSC Adv 5(43):34109–34116. https://doi.org/10.1039/C5RA04682C
Rahul AV, Santhanam M, Meena H, Ghani Z (2019) 3D printable concrete: Mixture design and test methods. Cem Concr Compos 97:13–23. https://doi.org/10.1016/j.cemconcomp.2018.12.014
Rao AP, Rao AV, Pajonk GM (2007) Hydrophobic and physical properties of the ambient pressure dried silica aerogels with sodium silicate precursor using various surface modification agents. Appl Surf Sci 253(14):6032–6040. https://doi.org/10.1016/j.apsusc.2006.12.117
Rosenthal M, Henneberger C, Gutkes A, Bues C-T (2018) Liquid Deposition Modeling: A promising approach for 3D printing of wood. Eur J Wood Prod 76(2):797–799. https://doi.org/10.1007/s00107-017-1274-8
Sandomierski M, Buchwald T, Strzemiecka B, Voelkel A (2020) Carbon black modified with 4-hydroxymethylbenzenediazonium salt as filler for phenol-formaldehyde resins and abrasive tools. J Appl Polym Sci 137(3):48160. https://doi.org/10.1002/app.48160
Sarmin SN (2016) The Influence of Different Wood Aggregates on the Properties of Geopolymer Composites. *Key Engineering Materials*, *723*, 74–79. https://www.scientific.net/KEM.723.74
Sarmin SN, Welling J, Krause A, Shalbafan A (2014) Investigating the Possibility of Geopolymer to Produce Inorganic-Bonded

Wood Composites for Multifunctional Construction Material – A Review. BioResources 9(4):7941–7950. https://ojs.cnr.ncsu.edu/index.php/BioRes/article/view/BioRes_09_4_Sarmin_Review_Investigating_Possibility_Geopolymer

Sayılkan H, Erdemoğlu S, Şener Ş, Sayılkan F, Akarsu M, Erdemoğlu M (2004) Surface modification of pyrophyllite with amino silane coupling agent for the removal of 4-nitrophenol from aqueous solutions. J Colloid Interface Sci 275(2):530–538. https://doi.org/10.1016/j.jcis.2004.02.009

Subasri R, Näfe H (2008) Phase evolution on heat treatment of sodium silicate water glass. J Non-cryst Solids 354(10):896–900. https://doi.org/10.1016/j.jnoncrysol.2007.08.037

Tang Y, Su H, Huang S, Qu C, Yang J (2017) Effect of Curing Temperature on the Durability of Concrete under Highly Geothermal Environment. *Advances in Materials Science and Engineering*, *2017*, e7587853. https://doi.org/10.1155/2017/7587853

Tran TT, Kang H, Kwon H-M (2019) Effect of Heat Curing Method on the Mechanical Strength of Alkali-Activated Slag Mortar after High-Temperature Exposure. Materials 12(11):1789. https://doi.org/10.3390/ma12111789

Ukaji E, Furusawa T, Sato M, Suzuki N (2007) The effect of surface modification with silane coupling agent on suppressing the photo-catalytic activity of fine TiO2 particles as inorganic UV filter. Appl Surf Sci 254(2):563–569. https://doi.org/10.1016/j.apsusc.2007.06.061

Valadez-Gonzalez A, Cervantes-Uc JM, Olayo R, Herrera-Franco PJ (1999) Chemical modification of henequén fibers with an organosilane coupling agent. Compos Part B: Eng 30(3):321–331. https://doi.org/10.1016/S1359-8368(98)00055-9

Vasconcelos GC, Santos TFA, Angrizani CC, Sales LA, Costa ML, Botelho EC (2021) Creep and Aging Evaluation of Phenol–Formaldehyde Carbon Fiber Composites in Overhead Transmission Lines. Appl Compos Mater 28:1697–1714. https://doi.org/10.1007/s10443-021-09935-6

Venet C, Vergnes B (2000) Stress distribution around capillary die exit: An interpretation of the onset of sharkskin defect. J Non-newton Fluid Mech 93(1):117–132. https://doi.org/10.1016/S0377-0257(00)00105-1

Vlachopoulos J, Strutt D (2003) The Role of Rheology in Polymer Extrusion. *Extrusion Minitec and Conference: From Basics to Recent Developments*, 20–21

Wang S-N, Zhang F-D, Huang A-M, Zhou Q (2016) Distinction of four Dalbergia species by FTIR, 2nd derivative IR, and 2D-IR spectroscopy of their ethanol-benzene extractives. *Holzforschung*, *70*(6), 503–510. https://doi.org/10.1515/hf-2015-0125

Whyman S, Arif KM, Potgieter J (2018) Design and development of an extrusion system for 3D printing biopolymer pellets. Int J Adv Manuf Technol 96(9–12):3417–3428. https://doi.org/10.1007/s00170-018-1843-y

Woern AL, Byard DJ, Oakley RB, Fiedler MJ, Snabes SL, Pearce JM (2018) Fused Particle Fabrication 3-D Printing: Recycled Materials' Optimization and Mechanical Properties. Materials 11(8):1413. https://doi.org/10.3390/ma11081413

Yang X, Zhu W, Yang Q (2008) The Viscosity Properties of Sodium Silicate Solutions. J Solution Chem 37(1):73–83. https://doi.org/10.1007/s10953-007-9214-6

Yoo D, Yoo B (2005) Rheology of Rice Starch-Sucrose Composites. Starch - Stärke 57(6):254–261. https://doi.org/10.1002/star.200400356

Zaharescu M, Predoana L, Pandele-Cusu J (2018) Thermal Analysis on Gels, Glasses, and Powders. In L. Klein, M. Aparicio, & A. Jitianu (Eds.), *Handbook of Sol-Gel Science and Technology: Processing, Characterization and Applications* (pp. 1833–1867). Springer International Publishing. https://doi.org/10.1007/978-3-319-32101-1_99

Zhou X, Yang J, Su D, Qu G (2009) The high-temperature resistant mechanism of α-starch composite binder for foundry. J Mater Process Technol 209(14):5394–5398. https://doi.org/10.1016/j.jmatprotec.2009.04.010

Zhu W, Aitken BG, Sen S (2017) Communication: Non-Newtonian rheology of inorganic glass-forming liquids: Universal patterns and outstanding questions. J Chem Phys 146(8):081103. https://doi.org/10.1063/1.4977085

Zuhua Z, Xiao Y, Huajun Z, Yue C (2009) Role of water in the synthesis of calcined kaolin-based geopolymer. Appl Clay Sci 43(2):218–223. https://doi.org/10.1016/j.clay.2008.09.003

Zuhua, Z., Xiao, Y., Huajun, Z., Yue, C. (2009). Role of water in the synthesis of calcined kaolin-based geopolymer. *Applied Clay Science*, *43*(2), 218–223. https://doi.org/10.1016/j.clay.2008.09.003

Supplementary Information The online version contains supplementary material available at https://doi.org/10.1007/s00107-022-01861-z.